



Interface engineering of polyaniline-functionalized porous Pd metallene for alkaline oxygen reduction reaction

Hongjing Wang, Wenxin Wang, Hongjie Yu*, Qiqi Mao, You Xu, Xiaonian Li, Ziqiang Wang*, Liang Wang*

State Key Laboratory Breeding Base of Green-Chemical Synthesis Technology, College of Chemical Engineering, Zhejiang University of Technology, Hangzhou 310014, PR China

ARTICLE INFO

Keywords:

Interface engineering
Pd metallene
Polyaniline modification
Electrocatalysis
Oxygen reduction reaction

ABSTRACT

Engineering the interface between two-dimensional materials and polymers is of great importance to improve their catalytic performance for oxygen reduction reaction (ORR). Hence, polyaniline (PANI)-functionalized porous Pd metallene (Pd@PANI metallene) is prepared via a two-step strategy. Due to the ultrathin porous nanosheets and interfacial structure, the Pd@PANI metallene possesses sufficient active sites and optimized electronic structure, which exhibits superior oxygen reduction performance in alkaline electrolyte. The mass and specific activities for Pd@PANI metallene are measured to $1.79 \text{ A mg}_{\text{Pd}}^{-1}$ and 2.96 mA cm^{-2} , which are 11.9 and 9.30 times those of Pt/C ($0.15 \text{ A mg}_{\text{Pd}}^{-1}$ and 0.32 mA cm^{-2}), respectively. Additionally, the ORR performance and morphology of Pd@PANI metallene can be maintained after long-term stability testing, making it an excellent ORR catalyst. This work provides an effective interface engineering strategy to construct efficient two-dimensional ORR electrocatalysts to improve the performance.

1. Introduction

Proton exchange membrane fuel cells (PEMFCs), as a class of sustainable energy conversion devices, have drawn extensive research because of their high energy density and no pollution [1–3]. Nevertheless, oxygen reduction reaction (ORR) with sluggish kinetics has severely hampered the large-scale implementation of PEMFCs. To date, Pt and Pt-based nanomaterials are still the dominant catalysts for ORR [4–7]. Nevertheless, limited reserves of Pt inevitably restrict its application in fuel cells [8–10]. Therefore, intensive efforts have been made to develop non-Pt electrocatalysts for ORR, including oxides [11], carbides [12,13], selenides [14], nitrides [15], transition metal-based sulfides [16–18], phosphides [19,20], as well as various carbon nanomaterials [21–23]. However, their intrinsic activity and long-term stability are far from those of Pt-based electrocatalysts. Recently, Pd as an active ORR catalyst has been extensively investigated to replace Pt in alkaline solutions [24–29]. Nonetheless, the slow electron transfer rate and weak binding energy of Pd to O cause the lower ORR performance [30,31]. As such, adjusting the surface electronic structure of Pd to improve the adsorption of strength for oxygenated species is highly desired.

Recently, a new class of ultrathin two-dimensional (2D) material consisting of bare metal elements in few atomic dimensions is referred to as a metallene, which have received ever-growing attention in sustainable energy conversion applications [24,32–37]. The metallene possesses high surface area, large surface energy, and tunable intrinsic electronic structures, which is beneficial for various electrocatalytic fields with outstanding catalytic activity [38,39]. To decrease the Pd usage and/or further improve intrinsic activity, interface engineering is considered as an effective way because it can promote electron transfer and influence the adsorption/desorption energies of adsorbed species in electrocatalytic reactions [40]. Polyaniline (PANI) has been considered as an attractive nanomaterial in various fields due to its high conductivity and stability, easy synthesis, environmentally friendliness, and good hydrophilicity [41,42]. Furthermore, the π -conjugated structure in PANI can promote the electrons transfer, regulate the electronic structure of nanomaterials and capture protons, thus regulating catalytic ability [43,44]. Previous studies have demonstrated that Pt/C@PANI displayed significantly enhanced ORR activity and stability compared to unmodified Pt/C catalysts due to electronic effect between the π -conjugated ligand in PANI and d orbitals of Pt [45]. In addition, the design of porous structure in 2D materials is also an effective method to

* Corresponding authors.

E-mail addresses: hongjieyu@zjut.edu.cn (H. Yu), zqwang@zjut.edu.cn (Z. Wang), wangliang@zjut.edu.cn (L. Wang).

<https://doi.org/10.1016/j.apcatb.2022.121172>

Received 7 December 2021; Received in revised form 13 January 2022; Accepted 31 January 2022

Available online 2 February 2022

0926-3373/© 2022 Elsevier B.V. All rights reserved.

construct high-performance electrocatalysts [46], which can provide more catalytically active sites and accelerated diffusion of electrolytes. However, the synthesis of the porous metallene is still a great challenge. Motivated by above consideration, it is expected that the rational interfacial design between porous metallene and PANI would provide an attractive idea to boost ORR performance.

Herein, we design and fabricate PANI-functionalized Pd metallene (Pd@PANI metallene) with active interfaces, which possesses highly porous, curved and ultrathin 2D nanosheet structure. The PANI functionalization can offer sufficient catalytically active sites, tunable surface electronic structure, and enhanced electrical conductivity for ORR. Therefore, the obtained porous Pd@PANI metallene exhibits excellent mass and specific activities in alkaline media, with 10.9 and 8.30 folds higher than those of commercial Pt/C, respectively, highlighting the significant role of the interface engineering between metal and polymer in the enhancement of ORR performance.

2. Experimental section

2.1. Materials and chemicals

Palladium (II) acetylacetonate ($\text{Pd}(\text{acac})_2$, 99%), aniline ($\geq 99.5\%$) and Nafion (5 wt%) were purchased from Sigma-Aldrich. Tungsten hexacarbonyl ($\text{W}(\text{CO})_6$, 97%), acetic acid (CH_3COOH , 99.5%), ammonium peroxydisulfate (APS, 98.0%), N,N-dimethylformamide (DMF, 99.5%), isopropanol (99.5%) and hydrochloric acid (AR) were purchased from Aladdin. Commercial Pt/C (20 wt%) and Pd/C (10 wt%) were ordered from Alfa Aesar.

2.2. Synthesis of porous Pd@PANI metallene

First, the porous Pd metallene was synthesized via solvothermal method. In a typical synthesis, $\text{Pd}(\text{acac})_2$ (10 mg) and $\text{W}(\text{CO})_6$ (20 mg) were ultrasonically dispersed in 8 mL of DMF. Then, 2 mL of acetic acid was added into the mixture solution, followed by heating to 50°C for 1 h. After cooling to room temperature, the product was washed and centrifuged with ethanol for several times, which was dispersed into water for further use. For PANI modification, 1 mL of 1.1 mM HCl and 1 mL of 13.4 mM aniline solution were dumped into 9 mL of Pd metallene solution (5 mg mL^{-1}) with stirring and sonication, and then maintained in an ice bath for 1 h. Afterwards, 1 mL of 13.4 mM APS was added to the mixture solution with stirring. After polymerization for 2 h, Pd@PANI metallene was obtained after washing and centrifugation for three cycles.

2.3. Characterizations

The microstructure of catalysts was observed from scanning electron microscopy (SEM, Zeiss Gemini 500) accompanied by energy dispersive X-ray spectroscopy (EDX) and transmission electron microscopy (TEM, Hitachi HT 7700). In addition, high-resolution TEM (HRTEM), high angle annular dark field scanning transmission electron microscopy (HAADF-STEM) and selected area electron diffraction (SAED) were operated on JEOL-2100F at a voltage of 300 kV. Atomic force microscope (AFM) was managed on Bruker Dimension ICON. The crystallographic data and surface electronic state of samples were investigated by X-ray diffractometer (XRD, PANalytical X'Pert) and X-ray photoelectron spectroscopy (XPS, ESCALAB MK II spectrometer), respectively. Fourier Transform Infrared Spectrometer (FTIR) measurement was performed by Nicolet iN10 (Thermo Scientific).

2.4. Electrochemical experiments

Electrocatalytic ORR measurements were carried out on CHI 852D electrochemical workstation equipping with a three-electrode system. A Pt wire and an Ag/AgCl (3 M KCl) electrode were employed to be the

counter electrode and reference electrode, respectively. The glassy carbon rotating disk electrode (RDE) modified with electrocatalysts was applied as working electrode. In brief, 2 mg of samples was dispersed in 1 mL water and Nafion mixed solution (v:v = 19:1) to form a homogeneous ink. Then, the RDE surface was spread with 2.5 μL of the above ink and dried. Before electrochemical tests, oxygen was passed into a 0.1 M KOH solution for saturation. Linear sweep voltammetry (LSV) was obtained at a scan speed of 10 mV s^{-1} in range of -0.9 to 0.2 V . Current density was normalized to the geometric area of the working electrode (0.071 cm^2) and all mentioned potentials were recorded with reversible hydrogen electrode (RHE). The kinetic current could be calculated based on the Koutecky-Levich (K-L) equation ($j_k = (j_d \times j)/(j_d - j)$, where j_k , j_d and j represent the kinetic current density, limited diffusion current density and measured current density, respectively). Electrochemical active surface area (ECSA) was measured by CO stripping tests. Firstly, CV curve was undertaken in 0.1 M CO-saturated HClO_4 solutions at a scan speed of 20 mV s^{-1} between 0 and 1.2 V. After removing CO from the solution by passing N_2 for 30 min, the CO stripping tests were still carried out at the same operation condition. The ECSA of samples was measured from the equation ($\text{ECSA} = Q/(m \times C)$, where Q , m and C represent the charge in the oxidation region of adsorbed CO, the Pd loading and the charge required for CO monolayer adsorption on the Pd surface ($420\text{ }\mu\text{C cm}^{-2}$), respectively). We tested electrochemical impedance spectroscopy (EIS) in 0.1 M KOH solution within the frequency range of 0.1 Hz to 100 kHz.

3. Results and discussion

3.1. Synthesis and characterization of Pd@PANI metallene

As illustrated in Fig. 1, the Pd@PANI metallene is obtained by a two-step synthetic approach. The Pd metallene is first prepared by a CO-confined growth strategy, in which the CO derived from $\text{W}(\text{CO})_6$ decomposition can act as a structure-directing agent. The CO could be strongly adsorbed on the (111) plane of Pd and limit its growth on the (111) plane, beneficial to the formation of 2D nanosheets [47–49]. As expected, the obtained sample exhibits an ultrathin nanosheet structure with highly well-defined curved characteristic, denoted as metallene (Fig. S1). Interestingly, the Pd metallene possesses rich porous structure, which may be derived from the release of adsorbed CO on Pd. The obtained Pd metallene was then used as precursor for the PANI modification *via in situ* chemical polymerization of aniline.

The Pd@PANI metallene retains the 2D nanosheet structure, indicating the universality of chemical polymerization for functionalization of 2D structure (Fig. S2). Typical HAADF-STEM and TEM images reveal the graphene-like structure of Pd@PANI metallene with large scale, in which the lateral size is measured to about 500 nm (Fig. 2a–c). Additionally, porous structures can be still observed in TEM image (Fig. 2d), indicating that the PANI modification cannot block the porous structures. From the folded border of Pd@PANI metallene, the thickness can be estimated to be approximately 1.3 nm (Fig. 2e), and the high-magnification TEM image exhibits that Pd metallene surface is covered by a thin amorphous PANI layer with the thickness of about 0.4 nm (Fig. 2f). These results are consistent with the analysis of atomic force microscopy (AFM) images (Fig. S3). The selected area electron diffraction (SAED) pattern with polycyclic morphology shows the polycrystalline features of the Pd@PANI metallene (Fig. S4). The microstructure of Pd@PANI metallene was further investigated by HRTEM in detail. Fig. 2g and 2h show that the Pd@PANI metallene possesses both amorphous and crystalline structures. The presence of the amorphous structure may be attributed to the slow nucleation and incomplete crystallization at low reaction temperature. The lattice fringes are revealed in apparent crystalline regions, with d -spacing of 0.225 nm, which correspond to the (111) plane of face-centered-cubic (fcc) Pd (Fig. 2h). As evident from elemental mapping images (Fig. 2i), Pd, C and N elements are evenly distributed in Pd@PANI metallene. The

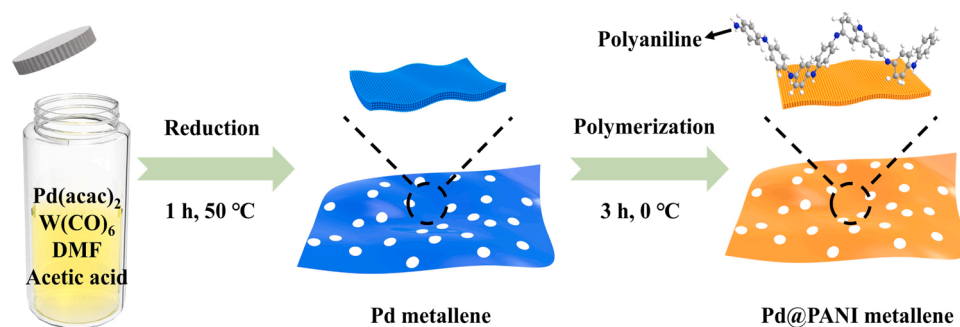


Fig. 1. The synthetic scheme of Pd@PANI metallene.

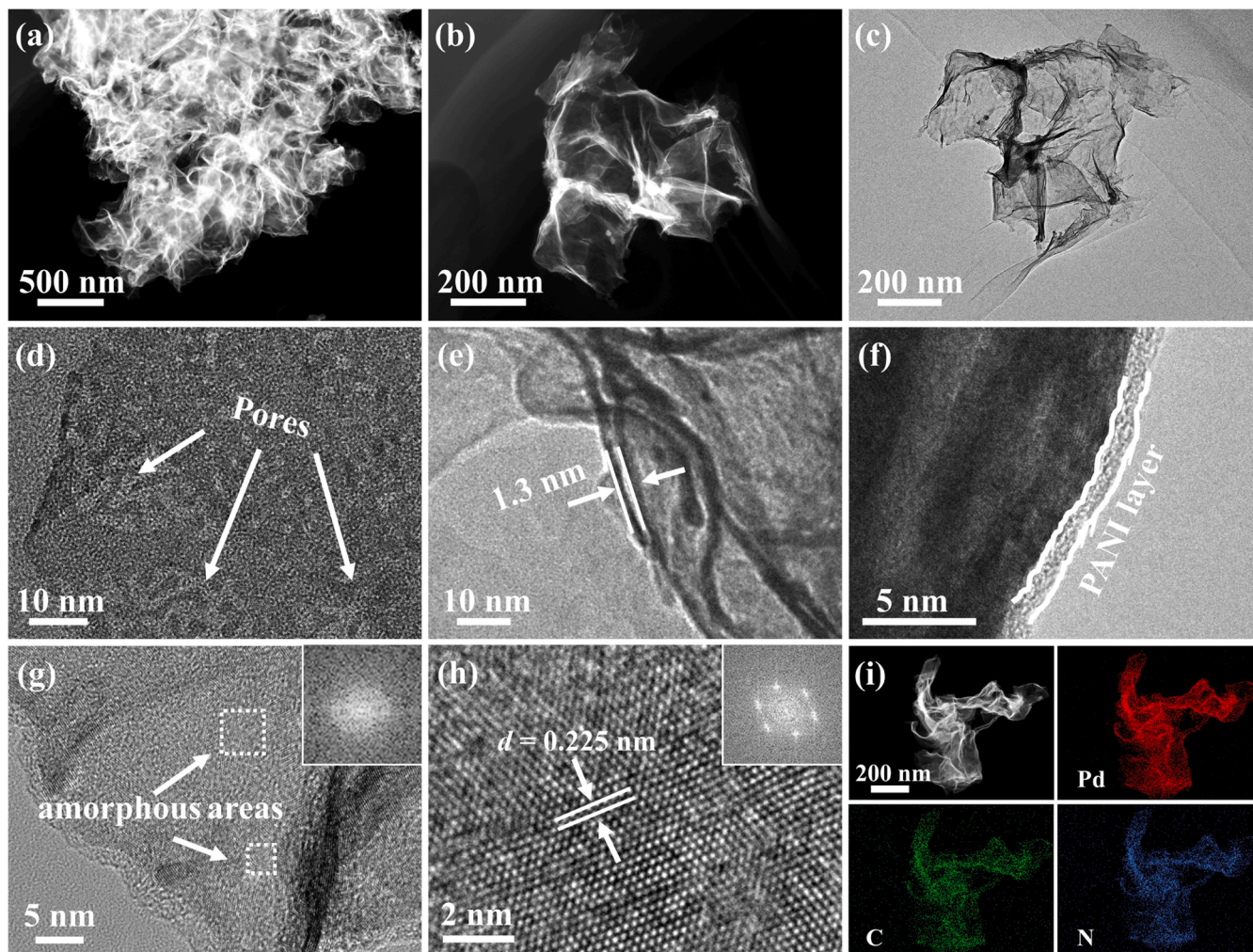


Fig. 2. (a and b) HAADF-STEM images, (c) low-magnification TEM image, (d–f) high-magnification TEM images, (g and h) HRTEM images of Pd@PANI metallene. (i) HAADF-STEM image and the corresponding elemental mappings of Pd@PANI metallene. The insets in (g) and (h) illustrate the corresponding FFT pattern of the selected areas.

weight ratio of Pd/C/N in the Pd@PANI metallene is measured to be 4.9/2.0/1.0 by EDX measurement, with the PANI content of approximately 38 wt% in sample (Fig. S5).

Next, the crystal structure of samples was characterized by XRD. The XRD pattern of Pd metallene shows four distinct diffraction peaks at 39.9° , 46.4° , 67.9° and 81.6° , corresponding to the (111), (200), (220) and (311) planes of the fcc Pd, respectively (Fig. 3a). After coating PANI layer, the XRD pattern of Pd@PANI metallene has no obvious changes of the position and intensity, indicating the formation of small amounts of

amorphous PANI layer on Pd surface. The molecular structure of PANI was demonstrated by FTIR spectrum (Fig. 3b), in which we can see several characteristic peaks of benzene ring C-H doubling zone (1717 cm^{-1}), C=C stretching of quinoid rings (1568 cm^{-1}), C=C stretching of benzoid units (1461 cm^{-1}), C=N stretching vibration of aromatic amines (1301 cm^{-1}) and aromatic amine C-H (1127 cm^{-1}) [45,50,51]. The surface composition and electronic structure of Pd@PANI metallene were analyzed by XPS. The XPS survey spectrum of Pd@PANI metallene confirms the existence of Pd, C and N elementals

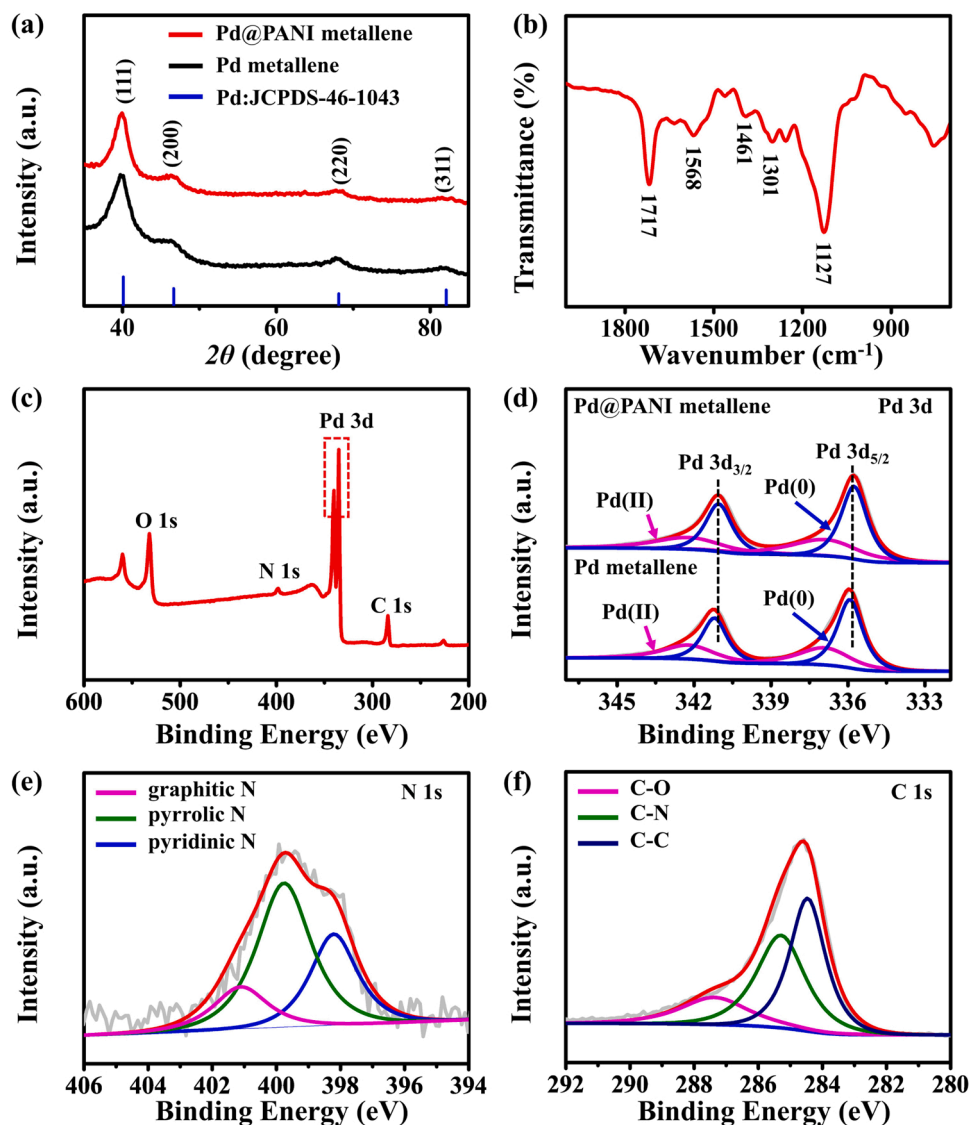


Fig. 3. (a) XRD patterns of the Pd@PANI metallene and Pd metallene. (b) FTIR spectrum and (c) XPS survey spectrum of Pd@PANI metallene. (d) XPS spectra of Pd 3d for the Pd@PANI metallene and Pd metallene. XPS spectra of (e) N 1s and (f) C 1s for the Pd@PANI metallene.

(Fig. 3c). As for the Pd 3d XPS spectra of Pd@PANI metallene (Fig. 3d), the peaks at 341.1 and 335.8 eV are attributed to $3d_{3/2}$ and $3d_{5/2}$ of Pd (0), respectively, and additional peaks at 342.5 and 337.0 eV are ascribed to Pd (II). Importantly, the Pd 3d peak of the Pd@PANI metallene shifts to a lower binding energy relative to those of Pd metallene because the nitrogen groups with high electron density can donate electron to Pd atom. This electronic interaction between Pd and PANI could cause an upshift of d -band center, which can result in the enhancement of the oxygen adsorption energy on Pd, thus improving the catalytic performance [43,52]. As for N 1s XPS spectra, the binding energies located at 401.1, 399.8 and 398.2 eV correspond to the graphitic N, pyrrolic N and pyridinic N species, respectively (Fig. 3e) [50,53]. According to peak areas, the Pd@PANI metallene mainly possesses the pyridine N and pyrrolic N species, which are beneficial for catalytic ORR via the four-electron pathway [54]. In addition, C 1s spectra of Pd@PANI metallene can be fitted to three peaks at 286.7, 284.7 and 283.9 eV, which can be divided into C—C, C—N, and C—O bonds, respectively (Fig. 3f) [55]. All above results confirm the successful modification of the PANI on Pd metallene.

3.2. ORR electroactivity of Pd@PANI metallene

We benchmarked the ORR performance of Pd@PANI metallene against Pd metallene, Pt/C and Pd/C under alkaline conditions (0.1 M KOH). The electrochemically active area (ECSA) is an important parameter for assessing catalyst activity, which is estimated from CO stripping experiments (Fig. S6). Based on the adsorption and desorption areas of CO, the calculated ECSA of Pd metallene is $57.6 \text{ m}^2 \text{ g}^{-1}$, much higher than that of Pt/C ($47.0 \text{ m}^2 \text{ g}^{-1}$) and Pd/C ($31.2 \text{ m}^2 \text{ g}^{-1}$), indicating that ultrathin, porous and highly curved 2D structure can provide sufficient catalytic active sites (Fig. S7). Moreover, the higher ECSA of Pd@PANI metallene ($60.5 \text{ m}^2 \text{ g}^{-1}$) is due to the presence of sufficient active interface sites by PANI modification [56,57], which can further promote ORR catalytic performance. Furthermore, the CV measurements of Pd@PANI metallene and Pd metallene were assessed in 1 M HClO₄ at a scan rate of 20 mV s^{-1} . The current peak related to the reduction of palladium oxide on Pd@PANI metallene exhibits a positive shift compared to that on Pd metallene (Fig. S8), revealing the higher potential required for the adsorption/desorption of hydroxyl groups on Pd@PANI metallene because the π -conjugated structure in PANI can optimize the electronic structure of Pd, which is beneficial to enhance ORR activity [58].

The ORR performance of all electrocatalysts was first investigated by LSV curves measured at 1600 rpm in O₂-saturated 0.1 M KOH solution (Fig. 4a). We can see from the LSV curves that the onset potential (E_{onset}) and half-wave potential ($E_{1/2}$) potentials of Pd@PANI metallene (1.02 and 0.97 V) are significantly higher than those of Pd metallene (1.01 and 0.95 V), Pt/C (0.96 and 0.87 V) and Pd/C (0.93 and 0.84 V) (Fig. 4b). The superior ORR activity of Pd@PANI metallene is because the isolated pyridine N species in PANI can donate electrons to O₂ and thus weaken the O-O bond, leading to the lower activation energy for ORR [50]. From the fitted LSV curve, the Tafel slope can be estimated, which is another worthwhile indicator to evaluate the ORR performance. The corresponding Tafel slopes for Pd@PANI metallene, Pd metallene, Pt/C and Pd/C are calculated to be 56.8, 66.4, 65.9 and 66.8 mV dec⁻¹ (Fig. 4c), respectively, revealing the faster ORR kinetics properties on Pd@PANI metallene due to fact that the strong electron-absorbing ability of N atoms in PANI can promote the oxygen adsorption on Pd. For the purpose of investigating the ORR mechanism, we conducted polarization curves of Pd@PANI metallene at various rotation rates from 625 to 2025 rpm (Fig. S9). The corresponding Koutecky-Levich plots of all samples show nearly overlapped, revealing their first-order reaction kinetics for the ORR. Furthermore, the electron transfer number (n) values for Pd@PANI metallene are estimated to 3.89, 3.86, 3.92 and 3.91 at 0.4, 0.5, 0.6 and 0.7 V from the slope, respectively, indicating the four-electron ORR pathway for the direct conversion of O₂ to OH⁻ by Pd@PANI metallene. The mass activity (MA) and specific activity (SA) are obtained by normalizing the kinetic current density to ECSA and Pd loading. The MA and SA values for the Pd@PANI metallene are 1.79 mA $\mu\text{g}_{\text{Pd}}^{-1}$ and 2.96 mA cm⁻² at 0.9 V, respectively, which are significantly better than those of Pd metallene (0.31 mA $\mu\text{g}_{\text{Pd}}^{-1}$ and 0.53 mA cm⁻²), Pt/C (0.15 mA $\mu\text{g}_{\text{Pt}}^{-1}$ and 0.32 mA cm⁻²) and Pd/C (0.065 mA $\mu\text{g}_{\text{Pt}}^{-1}$ and 0.21 mA cm⁻²) (Fig. 4d). The MA and SA values of the Pd@PANI metallene are also higher than those of most other reported Pd-based catalysts (See Table S1). These results suggest that the PANI modification on Pd surface has significant effect on the enhancement of ORR activity due to the increased oxygen adsorption energy on Pd and more active sites. In addition, electrochemical impedance (EIS) is

considered to be an effective approach to analyze the reaction and electron transfer kinetics at the electrode/solution interface. The Nyquist plots show the smallest charge transfer resistance (R_{ct}) for Pd@PANI metallene, which can be confirmed by the smallest the diameter of the semicircle (Fig. S10). More detailed data were obtained by fitting the impedance data to a simple equivalent circuit. The R_{ct} of Pd@PANI metallene is calculated to 314.8 Ω in an O₂-saturated 0.1 M KOH solution, smaller than those of Pd metallene (358.6 Ω), Pt/C (379.9 Ω) and Pd/C (426.1 Ω), revealing the higher conductivity of Pd@PANI metallene. This is because the π -conjugated ligand in PANI with high electron density can donate electrons to Pd atoms, thus enhancing electron transport rate of the catalyst.

3.3. ORR stability of Pd@PANI metallene

The stability and durability are also critical to the practical application of ORR electrocatalysts. The accelerated durability test (ADT) was performed by cycling the potential between 0.5 and 0.7 V in O₂-saturated 0.1 M KOH (Fig. 5a–c). After 10,000 CV cycles, the LSV curves exhibit little attenuation for Pd@PANI metallene but small decrease of $E_{1/2}$ values for Pd metallene (10.4 mV) and Pt/C (21.0 mV). Chronoamperometric measurements were further performed at 0.6 V for 5 h to study the durability of samples (Fig. 5d). The Pd@PANI metallene could maintain 92.32% relative current density after durability test, which is better than Pd metallene (90.27%) and Pt/C (79.21%). After the stability test, it can be shown by SEM, HAADF-STEM and TEM images that Pd@PANI metallene has no obvious change in morphology and structure (Fig. S11). The above results indicate the excellent stability of Pd@PANI metallene for the oxygen reduction process, which is mainly due to the large lateral size of metallene structure and the electronic interaction preventing the aggregation and dissolution of Pd.

The superior ORR performance of Pd@PANI metallene is highly related to the ultrathin porous 2D structure and PANI modification. The porous metallene can provide high surface area, sufficient active sites and large surface energy for oxygen reduction electrolysis. Furthermore, the surface modification of PANI layer can donate electrons to O₂ and

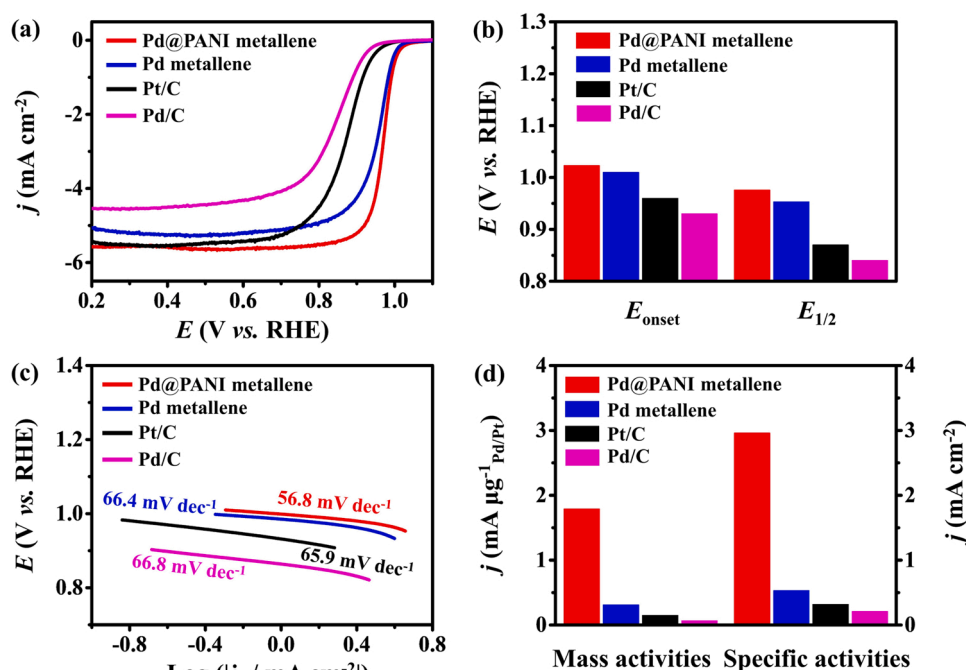


Fig. 4. (a) ORR polarization curves in an O₂-saturated 0.1 M KOH solution with a rotation rate of 1600 rpm at a scan speed of 10 mV s⁻¹ (b) The E_{onset} and $E_{1/2}$ for different samples. (c) Tafel slopes derived from polarization curves for the catalysts. (d) The comparison of mass activity and specific activity at 0.9 V for different samples.

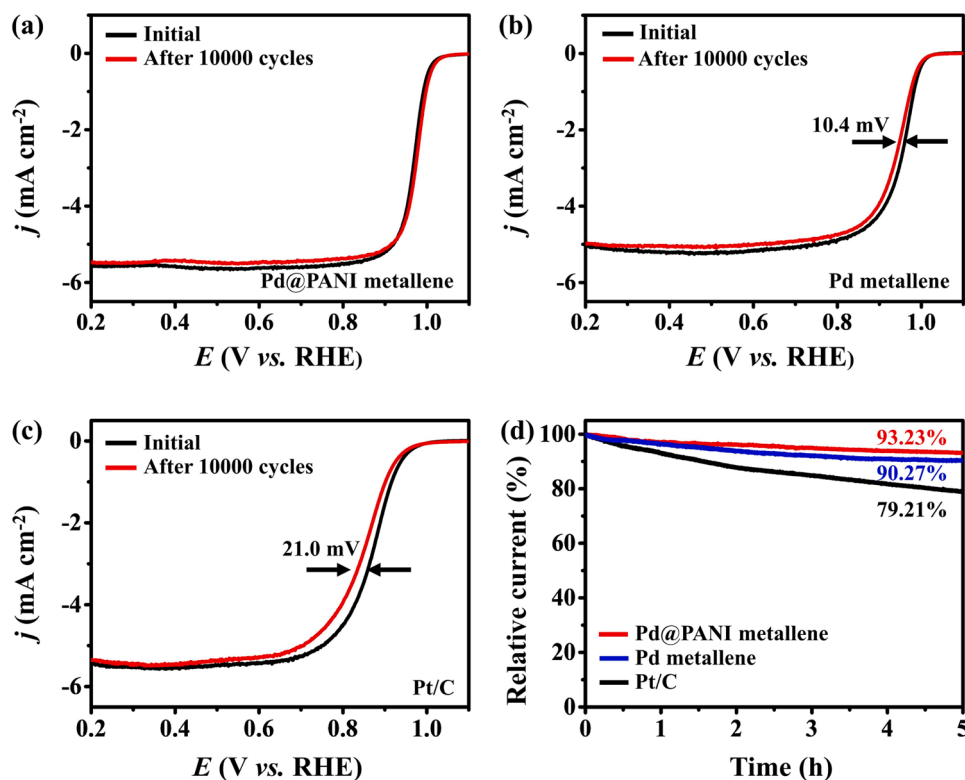


Fig. 5. ORR polarization curves of (a) Pd@PANI metallene, (b) Pd metallene and (c) Pt/C at a rotation rate of 1600 rpm and a scan rate of 10 mV s^{-1} before and after ADT test. (d) Chronoamperometric measurements of the catalysts at 0.6 V for 5 h in an O_2 -saturated 0.1 M KOH solution at a rotation rate of 1600 rpm.

thus weaken the O-O bond, leading to the lower activation energy for ORR. The strong electron-absorbing ability of N atoms can induce an upshift of d -band center of Pd, resulting in increased oxygen adsorption energy on Pd and the occurrence of the hydroxyl adsorption/desorption on Pd@PANI metallene at higher potentials, which is contributed to the enhancement of ORR performance. The pyridine N and pyrrolic N species of the PANI are beneficial for catalytic ORR via the four-electron pathway. In addition, the strong electronic effect can effectively prevent the aggregation and dissolution of Pd, leading to the excellent stability.

4. Conclusion

In summary, highly porous, curved and ultrathin Pd@PANI metallene has been successfully constructed by *in situ* chemical polymerization on Pd metallene. A range of electrochemical measurements show that Pd@PANI metallene possesses superior ORR activity and stability to Pd metallene and commercial Pt/C in alkaline media. The improved ORR electrochemical performance is contributed to more catalytically active sites, modulated electronic structure and enhanced conductivity by interface engineering between PANI and Pd metallene. It is believable that this surface functionalization by conductive polymer is a universal method for the preparation of high-performance catalysts with controllable shape and composition towards various electrocatalytic applications.

CRediT authorship contribution statement

Hongjing Wang: Writing – original draft, Writing – review & editing, Investigation, Formal analysis, Funding acquisition. **Wenxin Wang:** Writing – original draft, Writing – review & editing, Investigation, Formal analysis. **Hongjie Yu:** Formal analysis, Funding acquisition. **Qiqi Mao:** Visualization, Data curation. **You Xu:** Writing – review & editing. **Xiaonian Li:** Supervision. **Ziqiang Wang:** Writing – review &

editing, Supervision, Formal analysis, Funding acquisition. **Liang Wang:** Conceptualization, Writing – review & editing, Supervision, Funding acquisition.

Declaration of Competing Interest

The authors declare that they have no known competing financial interests or personal relationships that could have appeared to influence the work reported in this paper.

Acknowledgement

This work was financially supported by the National Natural Science Foundation of China (Nos. 21776255, 21972126, 21978264 and 21905250), China Postdoctoral Science Foundation (2021M702889), and Natural Science Foundation of Zhejiang Province (No. LQ22B030012).

Appendix A. Supporting information

Supplementary data associated with this article can be found in the online version at [doi:10.1016/j.apcatb.2022.121172](https://doi.org/10.1016/j.apcatb.2022.121172).

References

- [1] M.E. Scofield, H.Q. Liu, S.S. Wong, A concise guide to sustainable PEMFCs: recent advances in improving both oxygen reduction catalysts and proton exchange membranes, *Chem. Soc. Rev.* 44 (2015) 5836–5860, <https://doi.org/10.1039/c5cs00302d>.
- [2] R. Chattot, O. Le Bacq, V. Beermann, S. Kuhl, J. Herranz, S. Henning, L. Kuhn, T. Asset, L. Guetaz, G. Renou, J. Drnec, P. Bordet, A. Pasturel, A. Eychmüller, T. J. Schmidt, P. Strasser, L. Dubau, F. Maillard, Surface distortion as a unifying concept and descriptor in oxygen reduction reaction electrocatalysis, *Nat. Mater.* 17 (2018) 827–833, <https://doi.org/10.1038/s41563-018-0133-2>.
- [3] X.X. Wang, D.A. Cullen, Y.T. Pan, S. Hwang, M.Y. Wang, Z.X. Feng, J.Y. Wang, M. H. Engelhard, H.G. Zhang, Y.H. He, Y.Y. Shao, D. Su, K.L. More, J.S. Spendelov, G. Wu, Nitrogen-coordinated single cobalt atom catalysts for oxygen reduction in

- proton exchange membrane fuel cells, *Adv. Mater.* 30 (2018), 1706758, <https://doi.org/10.1002/adma.201706758>.
- [4] H. Doan, T. Morais, N. Borchtschoukova, Y. Wijsboom, R. Sharabi, M. Chatenet, G. Finkelshtain, Bimetallic Pt or Pd-based carbon supported nanoparticles are more stable than their monometallic counterparts for application in membraneless alkaline fuel cell anodes, *Appl. Catal. B: Environ.* 301 (2022), 120811, <https://doi.org/10.1016/j.apcatb.2021.120811>.
 - [5] Z.-N. Zhang, B.-Q. Miao, Z.-Q. Wu, P. Chen, X. Xiao, S.-N. Li, Y. Chen, Carbon nanobowl supported chemically functionalized PtRh nanocrystals: a highly active and methanol tolerant electrocatalyst towards the oxygen reduction reaction, *J. Mater. Chem. A* 9 (2021) 25621–25628, <https://doi.org/10.1039/d1ta08009a>.
 - [6] H. Wang, D. Yang, S. Liu, S. Yin, H. Yu, Y. Xu, X. Li, Z. Wang, L. Wang, Cage-bell structured Pt@N-doped hollow carbon sphere for oxygen reduction electrocatalysis, *Chem. Eng. J.* 409 (2021), 128101, <https://doi.org/10.1016/j.cej.2020.128101>.
 - [7] T.Y. Jeon, S.H. Yu, S.J. Yoo, H.Y. Park, S.K. Kim, Electrochemical determination of the degree of atomic surface roughness in Pt–Ni alloy nanocatalysts for oxygen reduction reaction, *Carbon Energy* 3 (2020) 375–383, <https://doi.org/10.1002/cey2.82>.
 - [8] Z. Wang, H. Zhang, S. Liu, Z. Dai, P. Wang, Y. Xu, X. Li, L. Wang, H. Wang, Engineering bunched RhTe nanochains for efficient methanol oxidation electrocatalysis, *Chem. Commun.* 56 (2020) 13595–13598, <https://doi.org/10.1039/d0cc05720g>.
 - [9] S. Yuan, J. Zhang, L. Hu, J. Li, S. Li, Y. Gao, Q. Zhang, L. Gu, W. Yang, X. Feng, B. Wang, Decarboxylation-induced defects in MOF-derived single Co atom@carbon electrocatalysts for efficient oxygen reduction, *Angew. Chem. Int. Ed.* 60 (2021) 21685–21690, <https://doi.org/10.1002/anie.202107053>.
 - [10] X. Xie, L. Peng, H. Yang, G.I.N. Waterhouse, L. Shang, T. Zhang, MIL-101-derived mesoporous carbon supporting highly exposed Fe single-atom sites as efficient oxygen reduction reaction catalysts, *Adv. Mater.* 33 (2021), 2101038, <https://doi.org/10.1002/adma.202101038>.
 - [11] X.P. Han, G.W. He, Y. He, J.F. Zhang, X.R. Zheng, L.L. Li, C. Zhong, W.B. Hu, Y. D. Deng, T.Y. Ma, Engineering catalytic active sites on cobalt oxide surface for enhanced oxygen electrocatalysis, *Adv. Energy Mater.* 8 (2018), 1702222, <https://doi.org/10.1002/aenm.201702222>.
 - [12] Y. Yu, J. Zhou, Z. Sun, Novel 2D transition-metal carbides: ultrahigh performance electrocatalysts for overall water splitting and oxygen reduction, *Adv. Funct. Mater.* 30 (2020), 2000570, <https://doi.org/10.1002/adfm.202000570>.
 - [13] X.-H. Yan, P. Prabhu, H. Xu, Z. Meng, T. Xue, J.-M. Lee, Recent progress of metal carbides encapsulated in carbon-based materials for electrocatalysis of oxygen reduction reaction, *Small Methods* 4 (2020), <https://doi.org/10.1002/smt.201900575> (1900575–294).
 - [14] Y. Zhang, Q. Zhou, J.X. Zhu, Q.Y. Yan, S.X. Dou, W.P. Sun, Nanostructured metal chalcogenides for energy storage and electrocatalysis, *Adv. Funct. Mater.* 27 (2017), 1702317, <https://doi.org/10.1002/adfm.201702317>.
 - [15] J.J. Jia, Z. Chen, Y.J. Liu, Y.F. Li, J.X. Zhao, RuN₂ monolayer: a highly efficient electrocatalyst for oxygen reduction reaction, *ACS Appl. Mater. Interfaces* 12 (2020) 54517–54523, <https://doi.org/10.1021/acsami.0c11824>.
 - [16] X.J. Shi, B.B. He, L. Zhao, Y.S. Gong, R. Wang, H.W. Wang, FeS₂-CoS₂ incorporated into nitrogen-doped carbon nanofibers to boost oxygen electrocatalysis for durable rechargeable Zn-air batteries, *J. Power Sources* 482 (2021), 228985, <https://doi.org/10.1016/j.jpowsour.2020.228985>.
 - [17] C. Han, Q. Li, D.W. Wang, Q.Q. Lu, Z.C. Xing, X.R. Yang, Cobalt sulfide nanowires core encapsulated by a N, S codoped graphitic carbon shell for efficient oxygen reduction reaction, *Small* 14 (2018), 1703642, <https://doi.org/10.1002/sml.201703642>.
 - [18] F. Liu, L. Zhang, L. Wang, F. Cheng, The electrochemical tuning of transition metal-based materials for electrocatalysis, *Electrochem. Energy Rev.* 4 (2021) 146–168, <https://doi.org/10.1007/s41918-020-00089-w>.
 - [19] V.V.T. Doan-Nguyen, S. Zhang, E.B. Trigg, R. Agarwal, J. Li, D. Su, K.I. Winey, C. B. Murray, Synthesis and X-ray characterization of cobalt phosphide (Co₂P) nanorods for the oxygen reduction reaction, *ACS Nano* 9 (2015) 8108–8115, <https://doi.org/10.1021/acsnano.5b02191>.
 - [20] C.S. Wang, W.B. Chen, D. Yuan, S.S. Qian, D.D. Cai, J.T. Jiang, S.Q. Zhang, Tailoring the nanostructure and electronic configuration of metal phosphides for efficient electrocatalytic oxygen evolution reactions, *Nano Energy* 69 (2020), 104453, <https://doi.org/10.1016/j.nanoen.2020.104453>.
 - [21] L. Du, G. Zhang, X. Liu, A. Hassanpour, M. Dubois, A.C. Tavares, S. Sun, Biomass-derived nonprecious metal catalysts for oxygen reduction reaction: the demand-oriented engineering of active sites and structures, *Carbon Energy* 2 (2020) 561–581, <https://doi.org/10.1002/cey2.73>.
 - [22] S. Li, Y. Wang, Y. Ding, Y. He, Y. Zhang, S. Li, J. Zhang, Y. Chen, Hollow N-doped carbon nanoflowers with nanosheets subunits for electrocatalytic oxygen reduction, *Chem. Eng. J.* 430 (2022), 132969, <https://doi.org/10.1016/j.cej.2021.132969>.
 - [23] L. Bai, Y. Zhang, W. Tong, L. Sun, H. Huang, Q. An, N. Tian, P.K. Chu, Graphene for energy storage and conversion: synthesis and interdisciplinary applications, *Electrochem. Energy Rev.* 3 (2019) 395–430, <https://doi.org/10.1007/s41918-019-00042-6>.
 - [24] H. Yu, T. Zhou, Z. Wang, Y. Xu, X. Li, L. Wang, H. Wang, Defect-rich porous palladium metallene for enhanced alkaline oxygen reduction electrocatalysis, *Angew. Chem. Int. Ed.* 60 (2021) 12027–12031, <https://doi.org/10.1002/anie.202101019>.
 - [25] D. Sun, Y. Wang, K.J.T. Livi, C. Wang, R. Luo, Z. Zhang, H. Alghamdi, C. Li, F. An, B. Gaskey, T. Mueller, A.S. Hall, Ordered intermetallic Pd₃Bi prepared by an electrochemically induced phase transformation for oxygen reduction electrocatalysis, *ACS Nano* 13 (2019) 10818–10825, <https://doi.org/10.1021/acsnano.9b06019>.
 - [26] J. Guo, L. Gao, X. Tan, Y. Yuan, J. Kim, Y. Wang, H. Wang, Y.J. Zeng, S.I. Choi, S. C. Smith, H. Huang, Template-directed rapid synthesis of Pd-based ultrathin porous intermetallic nanosheets for efficient oxygen reduction, *Angew. Chem. Int. Ed.* 60 (2021) 10942–10949, <https://doi.org/10.1002/anie.202100307>.
 - [27] F.D. Sanij, P. Balakrishnan, P. Leung, A. Shah, H. Su, Q. Xu, Advanced Pd-based nanomaterials for electro-catalytic oxygen reduction in fuel cells: a review, *Int. J. Hydrog. Energy* 46 (2021) 14596–14627, <https://doi.org/10.1016/j.ijhydene.2021.01.185>.
 - [28] T. Wang, A. Chutia, D.J.L. Brett, P.R. Shearing, G. He, G. Chai, I.P. Parkin, Palladium alloys used as electrocatalysts for the oxygen reduction reaction, *Energy Environ. Sci.* 14 (2021) 2639–2669, <https://doi.org/10.1039/d0ee03915b>.
 - [29] Z. Liu, X. Yang, B. Lu, Z. Shi, D. Sun, L. Xu, Y. Tang, S. Sun, Delicate topotactic conversion of coordination polymers to Pd porous nanosheets for high-efficiency electrocatalysis, *Appl. Catal. B: Environ.* 243 (2019) 86–93, <https://doi.org/10.1016/j.apcatb.2018.10.028>.
 - [30] L. Bu, C. Tang, Q. Shao, X. Zhu, X. Huang, Three-dimensional Pd₃Pb nanosheet assemblies: high-performance non-Pt electrocatalysts for bifunctional fuel cell reactions, *ACS Catal.* 8 (2018) 4569–4575, <https://doi.org/10.1021/acscatal.8b00455>.
 - [31] L. Bu, Q. Shao, Y. Pi, J. Yao, M. Luo, J. Lang, S. Hwang, H. Xin, B. Huang, J. Guo, D. Su, S. Guo, X. Huang, Coupled s-p-d exchange in facet-controlled Pd₃Pb tripods enhances oxygen reduction catalysis, *Chem* 4 (2018) 359–371, <https://doi.org/10.1016/j.chempr.2018.01.002>.
 - [32] P. Prabhu, J.M. Lee, Metalloenes as functional materials in electrocatalysis, *Chem. Soc. Rev.* 50 (2021) 6700–6719, <https://doi.org/10.1039/d0cs01041c>.
 - [33] J. Fan, J. Wu, X. Cui, L. Gu, Q. Zhang, F. Meng, B.H. Lei, D.J. Singh, W. Zheng, Hydrogen stabilized RhPdH 2D bimetallic nanosheets for efficient alkaline hydrogen evolution, *J. Am. Chem. Soc.* 142 (2020) 3645–3651, <https://doi.org/10.1021/jacs.0c00218>.
 - [34] X. Mu, J. Gu, F. Feng, Z. Xiao, C. Chen, S. Liu, S. Mu, RuRh bimetallic nanoring as high-efficiency pH-universal catalyst for hydrogen evolution reaction, *Adv. Sci.* 8 (2020), 2002341, <https://doi.org/10.1002/advs.2002341>.
 - [35] F. Lv, B. Huang, J. Feng, W. Zhang, K. Wang, N. Li, J. Zhou, P. Zhou, W. Yang, Y. Du, D. Su, S. Guo, A highly efficient atomically thin curved PdIr bimetallic nanosheet, *Natl. Sci. Rev.* 8 (2021) nwab019, <https://doi.org/10.1093/nsr/nwab019>.
 - [36] H. Xu, H. Shang, C. Wang, Y. Du, Recent progress of ultrathin 2D Pd-based nanomaterials for fuel cell electrocatalysis, *Small* 17 (2021), 2005092, <https://doi.org/10.1002/sml.202005092>.
 - [37] M.C. Luo, Z.L. Zhao, Y.L. Zhang, Y.J. Sun, Y. Xing, F. Lv, Y. Yang, X. Zhang, S. Hwang, Y.N. Qin, J.Y. Ma, F. Lin, D. Su, G. Lu, S.J. Guo, PdMo bimetallic nanosheet for oxygen reduction catalysis, *Nature* 574 (2019) 81–85, <https://doi.org/10.1038/s41586-019-1603-7>.
 - [38] Q. Dang, H. Lin, Z. Fan, L. Ma, Q. Shao, Y. Ji, F. Zheng, S. Geng, S.Z. Yang, N. Kong, W. Zhu, Y. Li, F. Liao, X. Huang, M. Shao, Iridium metallene oxide for acidic oxygen evolution catalysis, *Nat. Commun.* 12 (2021) 6007, <https://doi.org/10.1038/s41467-021-26336-2>.
 - [39] H.Q. Ta, R.G. Mendes, Y. Liu, X. Yang, J. Luo, A. Bachmatiuk, T. Gemming, M. Zeng, L. Fu, L. Liu, M.H. Rummeli, *In situ* fabrication of freestanding single-atom-thick 2D metal/metallene and 2D metal/metallene oxide membranes: recent developments, *Adv. Sci.* 8 (2021), 2100619, <https://doi.org/10.1002/advs.202100619>.
 - [40] Y.P. Zhu, C. Guo, Y. Zheng, S.-Z. Qiao, Surface and interface engineering of noble-metal-free electrocatalysts for efficient energy conversion processes, *Acc. Chem. Res.* 50 (2017) 915–923, <https://doi.org/10.1021/acs.accounts.6b00635>.
 - [41] J.F. Wu, Q.E. Zhang, J.J. Wang, X.P. Huang, H. Bai, A self-assembly route to porous polyaniline/reduced graphene oxide composite materials with molecular-level uniformity for high-performance supercapacitors, *Energy Environ. Sci.* 11 (2018) 1280–1286, <https://doi.org/10.1039/c8ee00078f>.
 - [42] Q. Dang, Y. Sun, X. Wang, W. Zhu, Y. Chen, F. Liao, H. Huang, M. Shao, Carbon dots-Pt modified polyaniline nanosheet grown on carbon cloth as stable and high-efficient electrocatalyst for hydrogen evolution in pH-universal electrolyte, *Appl. Catal. B: Environ.* 257 (2019), 117905, <https://doi.org/10.1016/j.apcatb.2019.117905>.
 - [43] H.C. Kim, Y. Kim, Y. Bando, Y. Yamauchi, J.W. Hong, Shape-controlled Pd nanocrystal–polyaniline heteronanostructures with modulated polyaniline thickness for efficient electrochemical ethanol oxidation, *J. Mater. Chem. A* 7 (2019) 22029–22035, <https://doi.org/10.1039/c9ta08349a>.
 - [44] J.X. Feng, S.Y. Tong, Y.X. Tong, G.R. Li, Pt-like hydrogen evolution electrocatalysis on PANI/CoP hybrid nanowires by weakening the shackles of hydrogen ions on the surfaces of catalysts, *J. Am. Chem. Soc.* 140 (2018) 5118–5126, <https://doi.org/10.1021/jacs.7b12968>.
 - [45] S. Chen, Z. Wei, X. Qi, L. Dong, Y.G. Guo, L. Wan, Z. Shao, L. Li, Nanostructured polyaniline-decorated Pt/C@PANI core-shell catalyst with enhanced durability and activity, *J. Am. Chem. Soc.* 134 (2012) 13252–13255, <https://doi.org/10.1021/ja306501x>.
 - [46] M. Zhang, Z. Wang, H. Yu, S. Wang, Y. Xu, X. Li, L. Wang, H. Wang, A mesoporous Au film with surface sulfur modification for efficient ammonia electrosynthesis, *J. Mater. Chem. A* 8 (2020) 20414–20419, <https://doi.org/10.1039/d0ta07305a>.
 - [47] L. Zhao, C. Xu, H. Su, J. Liang, S. Lin, L. Gu, X. Wang, M. Chen, N. Zheng, Single-crystalline rhodium nanosheets with atomic thickness, *Adv. Sci.* 2 (2015), 1500100, <https://doi.org/10.1002/advs.201500100>.
 - [48] L.Y. Zhang, Y. Ouyang, S. Wang, D. Wu, M. Jiang, F. Wang, W. Yuan, C.M. Li, Perforated Pd nanosheets with crystalline/amorphous heterostructures as a highly

- active robust catalyst toward formic acid oxidation, *Small* 15 (2019), 1904245, <https://doi.org/10.1002/sml.201904245>.
- [49] F. Gao, Y. Zhang, F. Ren, Y. Shiraishi, Y. Du, Universal surfactant-free strategy for self-standing 3D tremella-like Pd-M (M = Ag, Pb, and Au) nanosheets for superior alcohols electrocatalysis, *Adv. Funct. Mater.* 30 (2020), 2000255, <https://doi.org/10.1002/adfm.202000255>.
- [50] L. Yanhua, N. Tan, D. Huo, M. Ding, Y. Zhang, T. Liu, R. Yu, S. Cheng, R. Fan, Fabrication of porous N-rich carbon electrocatalysts from pyrolysis of PANI-encapsulated CeO₂ for enhanced oxygen reduction reaction, *J. Electrochem. Soc.* 168 (2021), 044516, <https://doi.org/10.1149/1945-7111/abf4ad>.
- [51] P. Najmi, N. Keshmiri, M. Ramezanzadeh, B. Ramezanzadeh, Synthesis and application of Zn-doped polyaniline modified multi-walled carbon nanotubes as stimuli-responsive nanocarrier in the epoxy matrix for achieving excellent barrier-self-healing corrosion protection potency, *Chem. Eng. J.* 412 (2021), 128637, <https://doi.org/10.1016/j.cej.2021.128637>.
- [52] A.L. Wang, H. Xu, J.X. Feng, L.X. Ding, Y.X. Tong, G.R. Li, Design of Pd/PANI/Pd sandwich-structured nanotube array catalysts with special shape effects and synergistic effects for ethanol electrooxidation, *J. Am. Chem. Soc.* 135 (2013) 10703–10709, <https://doi.org/10.1021/ja403101r>.
- [53] L. Yang, Y. Tang, D. Yan, T. Liu, C. Liu, S. Luo, Polyaniline-reduced graphene oxide hybrid nanosheets with nearly vertical orientation anchoring palladium nanoparticles for highly active and stable electrocatalysis, *ACS Appl. Mater. Interfaces* 8 (2016) 169–176, <https://doi.org/10.1021/acsami.5b08022>.
- [54] D. Guo, R. Shibuya, C. Akiba, S. Saji, T. Kondo, J. Nakamura, Active sites of nitrogen-doped carbon materials for oxygen reduction reaction clarified using model catalysts, *Science* 351 (2016) 361–365, <https://doi.org/10.1126/science.aad0832>.
- [55] C. Hu, L. Dai, Multifunctional carbon-based metal-free electrocatalysts for simultaneous oxygen reduction, oxygen evolution, and hydrogen evolution, *Adv. Mater.* 29 (2017), 1604942, <https://doi.org/10.1002/adma.201604942>.
- [56] J. He, M. Wang, W. Wang, R. Miao, W. Zhong, S.Y. Chen, S. Poges, T. Jafari, W. Song, J. Liu, S.L. Suib, Hierarchical mesoporous NiO/MnO₂@PANI core-shell microspheres, highly efficient and stable bifunctional electrocatalysts for oxygen evolution and reduction reactions, *ACS Appl. Mater. Interfaces* 9 (2017) 42676–42687, <https://doi.org/10.1021/acsami.7b07383>.
- [57] Z. Duan, K. Deng, C. Li, M. Zhang, Z. Wang, Y. Xu, X. Li, L. Wang, H. Wang, Polyaniline-coated mesoporous Rh films for nonacidic hydrogen evolution reaction, *Chem. Eng. J.* 428 (2022), 132646, <https://doi.org/10.1016/j.cej.2021.132646>.
- [58] Q. Xue, J. Bai, C. Han, P. Chen, J.-X. Jiang, Y. Chen, Au nanowires@Pd-polyethylenimine nanohybrids as highly active and methanol-tolerant electrocatalysts toward oxygen reduction reaction in alkaline media, *ACS Catal.* 8 (2018) 11287–11295, <https://doi.org/10.1021/acscatal.8b03447>.